Journal of Thermal Analysis and Calorimetry (2021) 145:2405–2416
https://doi.org/10.1007/s10973-020-09804-7

Physicochemical and thermal analysis of argan fruit residues (AFRs) as a new local biomass for bioenergy production

Yassine Rahib[1,2] · Brahim Sarh[1] · Jamal Chaoufi[2] · Sylvie Bonnamy[3] · Abdallah Elorf[1]

Received: 28 October 2019 / Accepted: 6 May 2020 / Published online: 26 May 2020

Abstract

A detailed investigation of the physicochemical properties and thermal characteristics of argan fruit residues (AFRs) was carried out to identify their potential application as biofuels. This experimental study covered the four main by-products of argan fruit: argan pulp (AP), argan nut shell (ANS), argan oilcake (AOC) and argan deoiled cake (ADC). Physicochemical analysis was performed to characterize biomass-based materials. Thermogravimetric techniques (TG, DTG and DTA) were applied to assess structural decomposition, biomass reactivity and combustion parameters. Lastly, thermal conductivity and diffusivity between 25 and 100 °C were measured using the transient plane source technique (TPS). The study shows that heating values were in the range of 17–22.5 MJ kg^{-1}, which is comparable to those of wood pellets and lignite coal. The maximum ash content was found in AP and the minimum in ANS. The residual oil of AOC was found to affect the drying process and calorific value. Thermal analysis showed that ANS has the highest ignition temperature and thermal conductivity values and therefore appears to be the most reactive material. Our data show that ANS has a good potential to produce heat through direct combustion. A pretreatment appears to be necessary to improve the characteristics of AP and AOC in order to make them suitable biofuels in the near future.

Keywords Argan fruit residues · Physicochemical analysis · Thermal analysis · Ignition temperature · Thermal conductivity

List of symbols

Roman letters

V	Volume (m^3)
M	Moisture (%)
HHV	Higher heating value (MJ kg^{-1})
NHV	Net heating value (MJ kg^{-1})
PD	Particle density (kg m^{-3})
BD	Bulk density (kg m^{-3})
ED	Energetic density (GJ m^3)
R	Reactivity (% min^{-1} $°C^{-1}$)
D	Ignition index
S	Combustion index
r	Rate (% min^{-1})
T	Temperature (°C)
t	Time (s)
TR	Temperature range (°C)
ρ_{pow}	Powder density (kg m^{-3})
ρ_{tr}	True density (kg m^{-3})

Greek letters

ρ	Density (kg m^{-3})
λ	Thermal conductivity (W m^{-1} K^{-1})
α	Thermal diffusivity (mm^2 s^{-1})

Subscripts

max	Maximal
i	Ignition
a	Average
b	Burnout

Abbreviations

AFRs	Argan fruit residues
AP	Argan pulp
ANS	Argan nut shell
AOC	Argan oilcake
ADC	Argan deoiled cake
TGA	Thermogravimetric analysis

✉ Yassine Rahib
yassine.rahib@cnrs-orleans.fr

[1] Institute of Combustion, Aerothermal, Reactivity and Environment (ICARE)-CNRS UPR3021, 45071 Orléans Cedex 2, France

[2] Laboratory of Electronics, Signal Processing and Modelling Physics, Department of Physics, Ibn Zohr University, 80000 Agadir, Morocco

[3] Laboratory of Confinement, Materials and Nanostructures (ICMN)-CNRS UMR7374, 45071 Orleans Cedex 2, France

DTG	Derivative of thermogravimetric
DTA	Differential thermal analysis
TPS	Transient plane source
VM	Volatile matter
FC	Fixed carbon
arb	As-received basis
db	Dry basis

Introduction

The use of alternative renewable energy sources has attracted considerable attention due to the risk of future energy insecurity and the environmental and sociopolitical issues linked with the use of fossil fuels. Due to their abundance worldwide, lignocellulosic biomasses (non-food materials) are considered as an important renewable alternative energy source. They offer the possibility to reduce the dependency on fossil fuels and contribute to reasonable economic and environment-friendly benefits [1]. It is expected that biomass energy research will lead to new local, regional, national and maybe international public–private partnerships for development [2].

Argan (Argania spinosa), a tree endemic to southwest Morocco, covers about 800,000 ha, representing more than 20 million trees. It is mainly cultivated for its oil and considered as an important socioeconomic resource for local populations [3]. The fruit comprises an external pulp and an extremely hard nut with two to three almonds from which a premium oil is pressed. Statistically, 38 kg of dried fruits gives 2.5 kg of almonds which are required to produce almost one liter of argan oil. Annual argan oil production is estimated at between 2500 and 4000 tons and generates large quantities of argan fruit residues (AFRs) [4].

To date, studies on AFRs have mainly focused on chemical characterization [5, 6] and mechanical properties (the case of ANS) [7]. Compared to other agricultural by-products, few studies have been carried out on the physicochemical characteristics and thermal analysis of AFRs for use as biofuels [8, 9]. In order to achieve the efficient conversion of AFRs, there is therefore a need to further understand their properties with a view to predicting their behavior. This can contribute to the proper design of several thermochemical conversion systems.

A detailed investigation of the physicochemical properties [10–15] and thermal analysis [16–20] of lignocellulosic biomass is of vital importance in biomass conversion processes. Using the transient plane source technique (TPS), Sjöström and Blomqvist [18] demonstrated the possibility of directly measuring the thermal properties of wood pellets at elevated temperatures. Zhu et al. [19] measured the thermal conductivity of cut tobacco by the TPS method in different conditions. Lönnermark et al. [20] investigated the thermal properties and self-heating propensity of different types of pellets. They demonstrated that the TPS technique was able to directly measure the thermal properties of bulk pellet material.

The main objective of the present study was to carry out for the first time an analytical characterization of argan biomasses in order to estimate their usefulness as energy source. In the first instance, physicochemical analyses were carried out. Thermal behavior was assessed by means of thermoanalytical techniques (TG, DTG and DTA). Lastly, thermal properties were evaluated, and the effect of elevated temperature was checked. A correlation between physicochemical properties, thermal conductivity and thermogravimetric combustion parameters was verified.

Materials and methods

Feedstock material

The AFRs used throughout this work were obtained from the Sousse-Massa region in Morocco. Photographs were taken for each residue as illustrated in Fig. 1. The studied biomasses were already naturally sun-dried in order to reduce moisture content. The argan nut shell (ANS) was separated from the rest of the almond. A conventional Soxhlet extraction apparatus was used to remove the residual oil from argan oilcake (AOC) using n-hexane as solvent. The sample thus produced will be named argan deoiled cake (ADC). Finally, the four biomass materials were ground in order to obtain homogenous samples.

Physical analysis

Before thermal analysis, the samples were analyzed to determine the main physical properties that affect thermal conversion. Proximate analysis was carried out using a Shimadzu DTG-60 analyzer according to the ASTM standard procedures D3173, D3174 and D3175 for moisture (M), ash and volatile matter (VM), respectively [21]. Fixed carbon (FC) content was obtained by difference from 100%. True density was assessed by the water immersion method while bulk density was assessed by measuring the mass of known volume of each biomass according to the CEN TS15103 method.

Chemical analysis

The ultimate analysis corresponding to the elemental composition of AFRs was performed using a FLASH 2000 CHNS/O analyzer (Thermo Scientific). The CHO index was

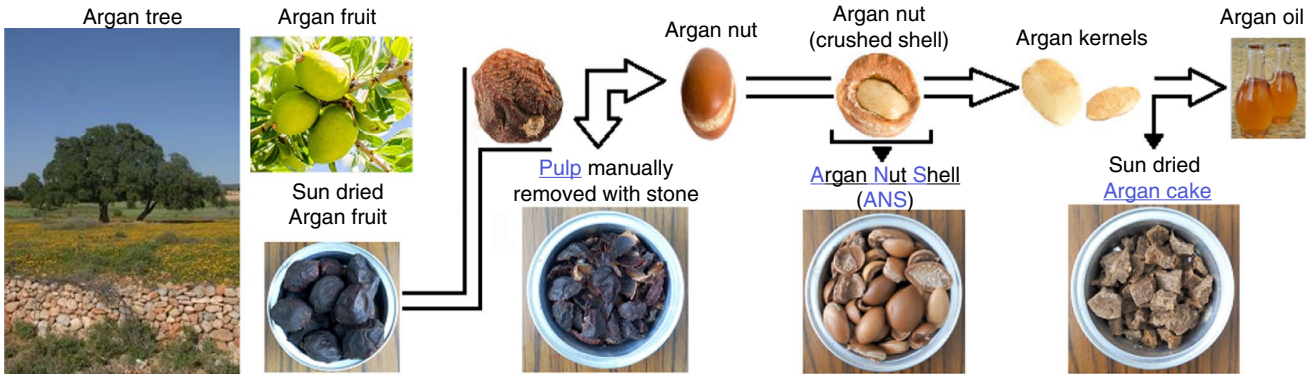

Fig. 1 Initial samples of AFRs obtained from a rural area in southwest Morocco

calculated as proposed by Mann et al. [22] to characterize the carbon oxidation potential according to the following formula:

$$\text{CHO } index = \frac{2 * [\text{O}] - [\text{H}]}{[\text{C}]} \quad (1)$$

where [O], [H] and [C] are the atomic amount of hydrogen, oxygen and carbon in a molecule, respectively.

The exact higher heating value (HHV) of AFRs on raw basis was measured using a PARR 1261 calorimetric bomb. The HHV on dry basis (HHV_{db}), the theoretical HHV based on the elemental composition and the net heating value (NHV) were also calculated [23].

Thermal analysis

Thermogravimetric analysis of AFRs was conducted to assess the structural decomposition behavior. TG and DTA experiments were performed in dynamic conditions using a Shimadzu DTG-60 analyzer at a heating rate of 10 °C min^{-1} from room temperature to 600 °C. Air and nitrogen gases with a constant flow of 20 mL min^{-1} were used to maintain the oxidative and the inert atmospheres, respectively.

The biomass reactivity (R) was defined as the decomposition rate of structural components during thermochemical conversion. This parameter was calculated based on the method proposed in previous investigations [9, 16, 24] by determining the maximum mass loss (DTG_{max}) and the corresponding temperature ($T_{DTG\ max}$) using the following equation:

$$R = 100 * \sum \frac{||DTG_{max}||}{T_{DTG\ max}} \quad (2)$$

Combustion parameters such as ignition and burnout temperature (T_i and T_b, respectively) and corresponding times (t_i and t_b) as well as the maximum rate of mass loss and corresponding time (r_{max} and t_{max}, respectively) were determined graphically from TG-DTG curves. T_i was determined according to the method defined by Li et al. [25] while T_b was defined when the DTG profile attained a 1% min^{-1} combustion rate. The average mass loss rate (r_a) was also determined. Finally, the ignition and combustion indices (D and S, respectively) were calculated according to the following formulae [25, 26]:

$$D = \frac{r_{max}}{t_{max} * t_i}; S = \frac{r_{max} * r_a}{T_i^2 * T_b} \quad (3)$$

Thermal properties of AFRs were measured using a hot disk thermal constant analyzer. The method is standardized (ISO22007-2) for measuring thermal conductivity (λ) and diffusivity (α) for all materials [27]. The measurement principle consists in imposing a uniform heat flux by placing a probe (sensor) between two samples, injecting a constant electric power and measuring the temperature variation in the samples [28]. The probe serves as a heat source and a temperature sensor (Fig. 2a, b). In this study, direct measurements of thermal conductivity and diffusivity of AFRs were made by introducing the sensor inside a cylindrical container filled with the studied biomass. Tests were carried out when the sensor was located both horizontally and vertically in the container to investigate the existence of sensor orientation effects (Fig. 2c, d). The samples were slightly compressed at the top of the container in order to achieve better adherence between the thermal sensor and the tested material.

The first part of the experiments was devoted to measuring the thermal conductivity of AFRs at room temperature by using the gray sensor (Fig. 2a). Low granulometry (≤ 0.5 mm) was chosen in order to access a correlation between thermal properties and thermal decomposition parameters. The second part of the experiments involved measuring the thermal properties between 25 and 100 °C using the red sensor (Fig. 2b). For this reason, a forced air oven was used to control and maintain the samples at the required temperature while their thermal properties were

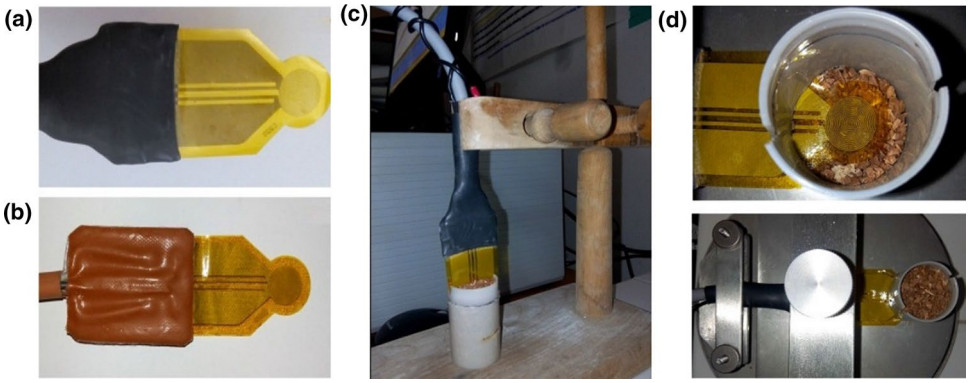

Fig. 2 Measuring methodology of thermal properties: (**a**) gray sensor, (**b**) red sensor, (**c**) and (**d**) vertical and horizontal locations of the TPS sensor, respectively

recorded. For all measurements at elevated temperatures, the sample was left at least 3 h in the oven to re-establish equilibrium. The assumption of measurement homogeneity and isotropy is satisfied since the sensor used is much larger than the individual crushed particles [18]. Repetition tests were conducted at least six times, and the mean values are reported.

Results and discussion

Physical analysis

Proximate analysis along with density analyses was carried out to characterize the studied materials. The results are shown in Table 1. For comparison purposes, other biomass (olive residues (OR), almond shell (AS) and olive wood (OW)) and coal samples (anthracite and lignite coal) have also been included [13, 29]. The results revealed that the moisture content of AFRs was in the range of 4.5–9.5%. These values are comparable with those of other biomass commonly used for biofuel applications (moisture content < 10%).

Biomass has a higher volatile matter (VM) than coal. This is an attractive feature for ignition performance and reactivity. The VM contents of AFRs ranged between 59 and 75%, which is comparable with literature results (Table 1). A fixed carbon/volatile matter (FC/VM) fuel ratio was calculated to characterize the combustibility of the studied materials. The fuel ratio of AFRs ranged from 0.21 (for AOC) to 0.41 (for

Table 1 Physicochemical composition of AFRs

Samples	Ref.	Proximate analysis/%, wet basis[a]				PD[a*]	BD[a*]	Ultimate analysis/%, wet basis[b]					HHV[a*]	NHV	ED
		M	VM	FC	Ash			C	H	N	O	S			
ANS	[9]	9.5	67.5	21.5	1.5	1060	596	51.33	6.32	0.005	42.345	n.d	18.3	17	10.13
AP	This work	8.5	59	24	8.5	1273	279	51.91	7.14	1.05	40.22	n.d	17.1	15.4	4.3
AOC	This work	5.5	74.5	15.5	4.5	1170	527	55.74	8.15	6.3	29.81	n.d	22.4	20.5	10.8
ADC	This work	10.5	67.5	16	6	–	–	50.47	7.23	8.34	33.96	n.d	19.3	17.6	–
OW	[13]	6.6	74.3	16.1	3	–	–	49	5.4	0.7	44.9	0.03	17[c, a]	–	–
OR	[13]	10.6	60.2	22.8	6.4	–	–	58.4	5.8	1.4	34.2	0.23	19.7[c, b]	–	–
AS	[13]	7.2	69.5	20.2	3.1	–	–	50.3	6.2	1	42.5	0.05	18.4[c, b]	–	–
AC	[29]	1.4	7.2	75.7	15.7	–	–	88.16	3.88	1.27	5.89	0.80	28.6[c, b]	–	–
LC	[29]	19.4	35.1	35.9	9.5	–	–	62.33	5.51	1.42	30.17	0.57	18.2[c, b]	–	–

M moisture, *VM* volatile matter, *FC* fixed carbon, *PD* particle density (kg m^{-3}), *BD* bulk density (kg m^{-3}), *HHV* high heating value (MJ kg^{-1}), *NHV* net heating value (MJ kg^{-1}), *ED* energy density (GJ m^{-3}), *n.d* not detected

OW olive wood, *OR* olive residues, *AS* almond shell, *AC* anthracite coal, *LC* lignite coal

[a]As-received basis, [b]dry ash-free basis, [c]calculated from elemental analysis, *assay was conducted in quadruplicate, and the mean value is reported

AP), i.e., a lower fuel power and a higher material reactivity than coal, which has an FC/VM ratio of 1.02 and 10.52 for lignite coal (LC) and anthracite coal (AC), respectively. Therefore, the combustion of AFRs will be dominated by the gas-phase oxidation of volatiles (flaming mode) [8, 30, 31]. The low fuel ratio of AOC (0.21) makes it easy to burn which requires prudent shipping and handling in summer because of its propensity to catch fire. Similarities between AOC and OW as well as between ANS and AS were observed.

Ash contents affect the combustion behavior of the fuel. In the samples analyzed here, the lowest ash content was found in ANS (1.5%) compared to other biomass (~3%) and coal (~10%). This indicates that using ANS as an alternative fuel could reduce the costs of ash disposal during combustion. For the AP biomass, with a high ash content, consideration must be given to ensuring successful ash removal.

An important characteristic of biomass materials is their energy density (ED) which was calculated from the NHV and bulk density (BD). It is worth noting that the high ED of ANS makes it an attractive material for energy production due to its low transportation costs [9].

Chemical analysis

Ultimate analyses were performed to determine the carbon, hydrogen, nitrogen, sulfur and oxygen content of AFRs. These key elements define fuel efficiency and are considered as the significant constituents of lignocellulosic biomass. The chemical composition results, on ash-free dry basis, of the studied biomasses are reported in Table 1. AFRs have a high carbon and hydrogen content compared to OW and AS. AOC is characterized by a lower oxygen and higher carbon content, after OR, compared to the other biomasses. The negligible sulfur content of AFRs favors clean combustion conditions. With respect to the nitrogen content, ANS has a practically negligible amount, and therefore, nitrogen oxide emissions will likely be minimal. The empirical formulae were $C_{1.62}H_{2.39}O$, $C_{57.3}H_{95.2}NO_{33.5}$, $C_{10.3}H_{18.1}NO_{4.14}$ and $C_{7.06}H_{12.03}NO_{3.56}$ for ANS, AP, AOC and ADC, respectively. They can be used in estimating the products produced by pyrolysis and combustion. The chemical composition results can be illustrated by a van Krevelen diagram based on the atomic ratio (Fig. 3). As can be seen, the coal materials have lower H/C and O/C atomic ratios than the biomass. Lower O/C and H/C ratios signify a higher energy content and more difficult combustion behavior. Thus, biomass is more reactive than coal. The lowest O/C atomic ratio was found in AOC, which explains its higher heating value. Similarities between the ANS and AS biomass were observed.

Figure 4 shows the oxidation state of the carbon content (CHO index) in the studied fuels. The CHO index values of biomasses ranged from − 0.95 to − 0.12, except for OW that has an index of + 0.05 which denotes a much higher oxygen content and lower amount of hydrogen. The CHO index values of coal samples are relatively close (− 0.33 and − 0.43 for LC and AC, respectively). From this study, AOC appears to be the most reduced molecule while ANS is the most oxidized one.

The HHV of AFRs on as-received basis was estimated using a Parr oxygen bomb calorimeter. The results ranged from 17.1 to 22.37 MJ kg^{-1} (Fig. 5). These values are in the same order of magnitude as the results obtained for olive wood, olive residues and almond shell (Table 1). Comparison with the literature data shows that the AFRs have a typical energy content. HHVs were also estimated by taking ultimate analysis data into account. The theoretical HHVs were consistent with the experimental values with an estimated average relative error of 4%.

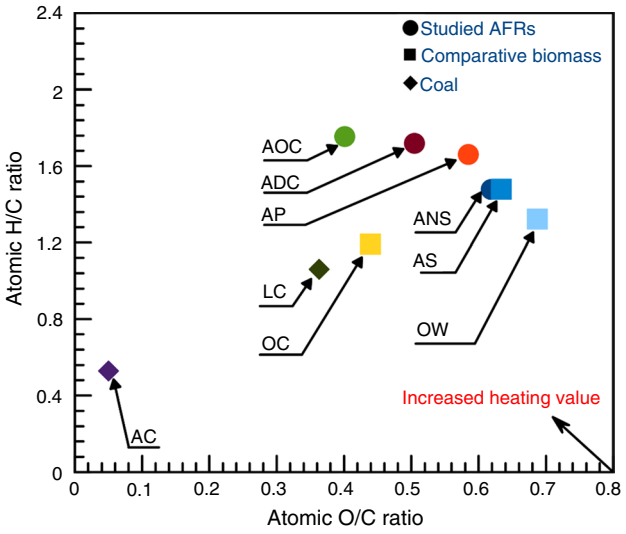

Fig. 3 van Krevelen plot. The results of the other fuels are included [13, 29]

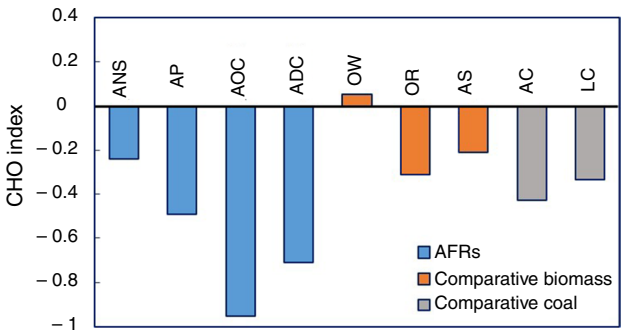

Fig. 4 CHO index of AFRs compared to other fuels (Data adapted from Refs. [13, 29])

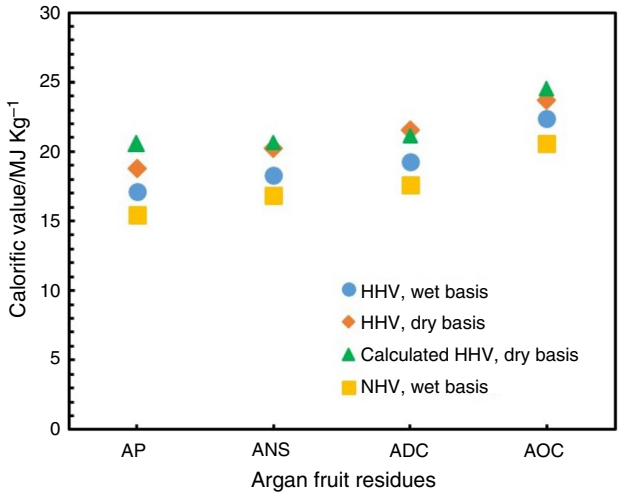

Fig. 5 Calorific value of AFRs

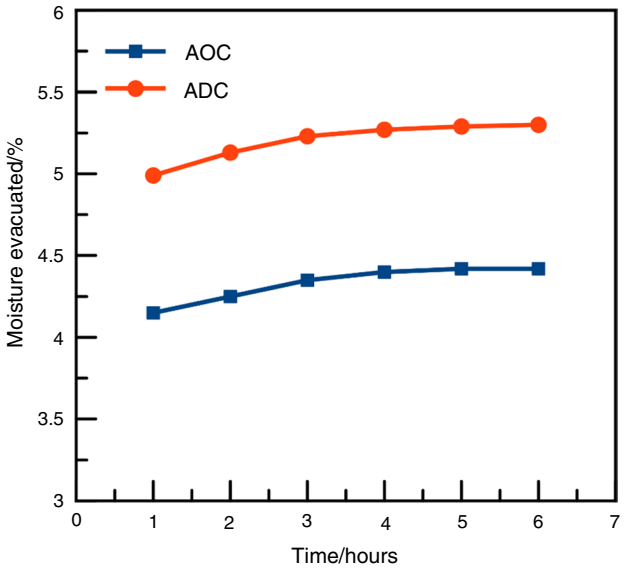

Fig. 6 Drying of AOC and ADC at stable temperature of 80 °C

The residual oil in biomass affects their physicochemical characteristics and combustion products. To determine the oil content, a solid/liquid extraction was set up using a Soxhlet extractor. The tests were conducted in triplicate, and the mean value of oil content in the sun-dried AOC was found to be 18%. This high quantity appears to be due to the manual method of oil extraction. Residual oil of argan cake was found to influence both the drying process and the energy content. Figure 6 compares the drying process at stable temperature of 80 °C in argan cake before and after oil extraction. It can be seen that ADC evacuates a much higher moisture content (5.3%) than AOC (4.4%) which means that ADC soaks up more moisture. This can be seen also from the results of moisture content in proximate analysis (Table 1). Residual oil within AOC prevents the water from rising to the surface of the material and thus influences moisture evacuation. This behavior was also reported by Koukouch et al. [32] in their study of the drying of olive pomace waste. Both the surplus of moisture and the loss of residual oil content contribute to decreasing the energy content. The results in Fig. 5 show that AOC has a high HHV value (23.7 MJ kg^{-1}). A total extraction of residual argan oil from the cake entails a decrease in the HHV value (21.54 MJ kg^{-1}) which can be explained by the high heating value of argan oil (39.3 MJ kg^{-1}) [33]. Despite this decrease, the measured value remains high enough for energy purposes.

Thermal analysis

Thermal characteristics under pyrolysis conditions

The TG and the corresponding DTG and DTA curves of AFRs are shown individually in Fig. 7a–c. Our findings reveal that the pyrolysis of AFRs presents two domains (Fig. 7a, b). The first mass loss (20–133 °C) is associated with the release of moisture. Seemingly, the higher DTG_{peak} of ANS (2.5% min^{-1}) was due to both the high water content and the low temperature of moisture release. The pyrolytic stages (second mass loss) for ANS, AP, AOC and ADC started at approximately 231, 132, 166 and 165 °C and finished at around 415, 363, 464 and 434 °C, respectively. During this stage, the decomposition of hemicellulose and cellulose is assumed to have taken place. For ANS, AP and AOC, two separate peaks were identified on the DTG curves. The first peak, which represents the thermal decomposition of the hemicelluloses, is located at the anticipated temperatures of 287, 205 and 325 °C for ANS, AP and AOC, respectively. The second peak incorporates the thermal degradation of cellulose and the residual part of lignin and is observed at the temperature of 361, 282 and 381 °C for the same biomass sequence. The decomposition of cellulose from the AP and the initial decomposition of AOC appear as a pronounced shoulder which means, in the case of AP, a lower cellulose content [34] and for AOC the initiation of hemicellulose degradation. The thermal decomposition of ADC displayed one homogenous region with a maximum DTG peak located at 318 °C. At the end, the remaining mass was 22.6, 32.4, 20 and 22.1% for ANS, AP, AOC and ADC, respectively.

DTA curves of AFRs during pyrolysis reveal that endothermic reactions dominate over exothermic reactions in the studied temperature range (Fig. 7c). The first peaks due to dehydration occurred between the temperatures of 25 °C and 100 °C with a maximum of 59, 48 and 44 °C for ANS, AP and ADC, respectively. The AOC did not show this peak because of the low moisture content. Above 100 °C, all

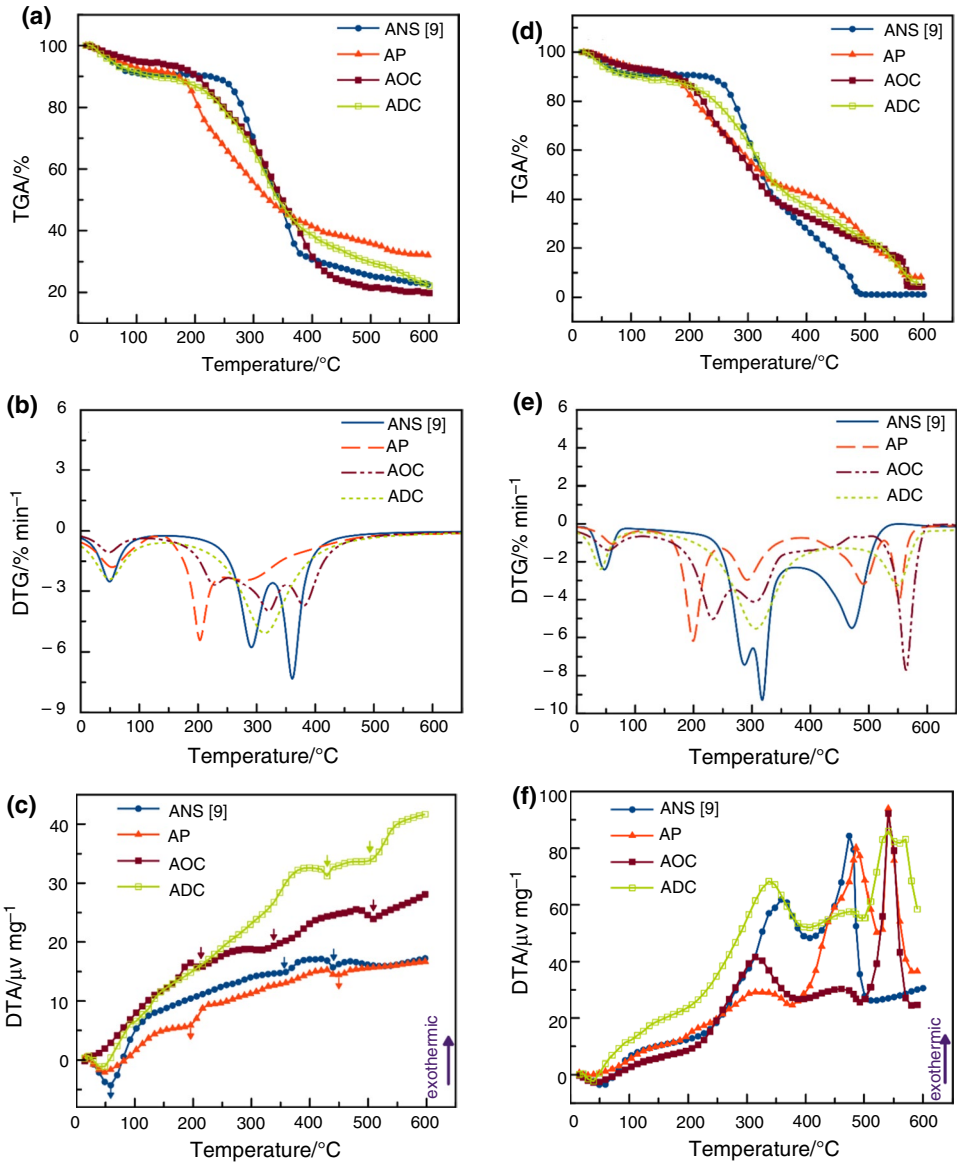

Fig. 7 Thermogravimetric analysis of AFRs: (**a**), (**b**) and (**c**) shows TG, DTG and DTA profiles during pyrolysis, respectively. (**d**), (**e**) and (**f**) display TG, DTG and DTA profiles during combustion, respectively

the AFRs show different endothermic peaks (illustrated by arrows in Fig. 7c) indicating the degradation of hemicellulose, cellulose and a small portion of lignin. Thus, pyrolysis of AFRs was dominated by the decomposition of cellulose components and volatilization.

The reactivity values of AFRs were found to decrease in the order of ANS (3.95) < AP (3.43) < AOC (3.09) < ADC (1.06% min^{-1} $°C^{-1}$). ANS appears to be the most reactive material compared to the other AFRs.

Thermal characteristics under atmospheric air conditions

Figure 7d-e shows the TG-DTG curves of AFRs under oxidative atmosphere. It was observed that after moisture removal the mass loss occurs in two main steps: The first one corresponds to the release of volatile matter leading to the formation of char, and the second one relates to the oxidation reactions. The remainder, at the end of combustion, called residual ash, was about 1.5, 8.5, 4.5 and 6% for ANS, AP, AOC and ADC, respectively. Thermal decomposition behaviors are usually explained by the lignocellulosic composition of biomass residues, where hemicellulose cellulose and lignin are the main components. From the extensive literature on the thermal behavior of biomasses, it was observed that the decomposition of hemicellulose, cellulose and lignin is completed in the temperature ranges 210–325, 310–400 and 160–900 °C, respectively [35, 36]. The drying process of AFRs ranges from ambient temperature to 120 °C. ANS and ADC show the highest mass loss rate peaks during this stage. The fast pyrolysis step took place between 148

and 388 °C (Table 2). This step was characterized by two decomposition processes for ANS, AP and AOC. The first, occurring between 150 and 300 °C, was related to the thermal depolymerization of hemicellulose. The second one, observed between 250 and 388 °C, was attributed to the thermal degradation of cellulose [30, 35]. The pyrolysis of ADC shows a single homogenous peak between 175 and 378 °C, indicating the thermal degradation of hemicellulose and cellulose, but also partially that of lignin. After the pyrolysis of AFRs, a significant fraction of char remained. This fraction was oxidized in the second stage, where the lignin was mostly decomposed. As evidenced in Fig. 7d, e, this stage takes place between 380 and 590 °C and has a single peak, apart from AP which exhibits a more complex process. Char oxidation from AOC and ADC requires a high temperature to proceed. These two materials exhibited a steady zone between 360 and 510 °C which results in shifting the reaction peak to the high temperature zone. The temperature ranges of char oxidation were 508–595 °C and 507–581 °C for AOC and ADC, respectively. This behavior can be explained from the results of the elementary analysis. The AOC and ADC molecules have a low CHO index (reduced oxygen molecules). Therefore, the last stage of thermal degradation will begin later at high temperatures.

In terms of biomass reactivity, the ANS appeared to be the most reactive material while ADC was the least reactive. This can be explained by the fact that the hemicellulose and cellulose components of ANS are high compared to its lignin content [37].

Combustion parameters can be employed to evaluate the relative combustion properties of AFRs. As shown in Table 3, AP has the lowest ignition temperature (T_i) while ANS has the highest. AOC has a relatively higher burnout temperature (T_b), indicating its poorer combustibility than that of the other materials studied. Moreover, ANS displayed a better ignition performance and high combustion reactivity.

The DTA curves obtained during combustion indicate various endothermic and exothermic reactions (Fig. 7f). Endothermic peaks between 20 and 120 °C correspond to the evacuation of water. The first exothermic peak occurred between 190 and 407 °C. In this temperature interval, thermal degradation is largely due to the pyrolysis of hemicellulose, cellulose and partly that of lignin. The second exothermic peak ranged between 480 and 570 °C and is attributed to the oxidation stage of AFRs. This peak shows an intense signal compared to the first one. These results are consistent with those revealed by the DTG curves in Fig. 7e. It is worth mentioning that the DTA curves of AOC and ADC exhibit the same behavior as the DTG curves concerning the steady zone before the oxidation of char.

Thermal properties

Thermal conductivity (λ) and thermal diffusivity (α) are of vital importance in understanding the thermochemical conversion processes of biomass fuels and their stability during storage [18, 38, 39]. The measured λ of AFRs at ambient conditions is shown in Fig. 8a. As is evident from this figure,

Table 2 Characteristics of oxidative thermogravimetric analysis

Samples	Devolatilization zone				Char combustion zone				*R*
	TR/°C	DTG_{max}/% min^{-1}	T_{peak}/°C	$DTG_{average}$/% min^{-1}	TR/°C	DTG_{max}/% min^{-1}	T_{peak}/°C	$DTG_{average}$/% min^{-1}	
ANS [9]	207–301 301–387	7.38 9.23	287 317	6.77	387–531	5.54	481	4.92	6.63
AP	149–253 253–375	6.18 3.1	201 290	1.55	386–529 529–575	3.04 4.13	490 549	2.75	5.52
AOC	151–268 268–361	4.84 4.15	235 308	4.22	508–595	7.6	562	1.30	4.76
ADC	175–378	5.43	306	3.85	507–581	3.26	547	3.12	2.36

R biomass reactivity (% min^{-1} C^{-1})

Table 3 Combustion parameters of AFRs

Sample	T_i/°C	T_{max}/°C	T_b/°C	t_i /min	t_b/min	r_a/% min^{-1}	r_{max}/% min^{-1}	t_{max}/min	*D*	$S*10^7$
ANS [9]	253	317	525	23.5	48	2.8	9.2	29.2	0.0134	7.60
AP	175	201	583	15.5	55.8	0.8	6.2	29.2	0.0128	2.78
AOC	187	562	595	16.5	56.8	1.6	7.6	51.4	0.009	5.73
ADC	228	306	581	21	55.7	1.8	5.4	28.3	0.0091	3.18

there is no significant difference between measurements performed with the horizontal or vertical orientation of the probe. The slight variation observed is likely due to the effect of heterogeneities which cannot be utterly neglected if the probe location is changed. Room temperature conductivity was 0.153, 0.134 and 0.113 W m^{-1} K^{-1} for ANS, AOC and AP, respectively. A good repeatability of the experiments was demonstrated by means of standard deviation (±0.002 W m^{-1} K^{-1}). The measured thermal conductivity of ANS was found to be consistent with that measured by Tatane et al. [40]. As the temperature increases, λ values increase up to 60 °C for ANS, and 80 °C for AP and AOC. Afterwards, λ values show a decreasing trend (Fig. 8.b). Concerning thermal diffusivity (α) data, the AP is in the interval of 0.106 to 0.130 mm^2 s^{-1}. The AOC decreases from 0.127 and stabilizes at ~ 0.114 mm^2 s^{-1} from 40 to 100 °C. For ANS, a decreasing trend from 0.183 to 0.117 mm^2 s^{-1} was observed (Fig. 8c). This means that with increasing temperature the transmitted energy rate and the surface heating effect of ANS become lower. The initial increase in conductivity with temperature is a familiar behavior for biomass insulating material [18, 19, 38, 41]. The different trend above 80 °C (for ANS) and 100 °C (for AP and AOC) was most likely due to vaporization. Water is more conductive (0.613 W m^{-1} K^{-1} at 300 K) and has a higher heat capacity than biomass [42]. Vaporization therefore reduces the λ values of the studied samples since the configuration properties and density within the materials are modified. The results of thermal properties behavior as a function of elevated temperature were found to be consistent with those of wood pallets studied by Sjöström and Blomqvist [18].

The thermal degradation behavior of biomass is commonly clarified by the effect of density and thermal conductivity which possess the highest sensitivity among the other physical properties. During the combustion of wood waste furniture, Khalfi et al. [43] found that biomass samples having a lower conductive heat transfer and bulk density (BD) ignite faster than those with a high λ and BD and may exhibit a lower rate of combustion. This behavior was also reported by El May et al. [16] in their study of the combustion behavior of date palm residues. Moreover, Mansaray and Ghaly [17] found that biomass fuels with a higher percentage of ash in their composition have a lower initial degradation temperature.

Figure 9a–c reports the most pertinent results of the thermophysical characterization. Figure 9a shows that AP with lower λ and BD values ignites faster (T_i = 175 °C) than AOC (T_i = 187 °C) and ANS (T_i = 253 °C). The ANS characterized by high λ and BD values shows a high rate of combustion (DTG_{max} = 9.23% min^{-1}) compared to AOC and AP (7.6 and 6.18% min^{-1}, respectively) as illustrated in Fig. 9b. This can be explained by the fact that during the heating of AP, a specific temperature gradient is produced, leading to heat transfer restrictions within the biomass material. The heat flux is not transmitted efficiently through AP and accumulates on the open surface. At that point, the temperature increases swiftly which leads to a very short ignition time.

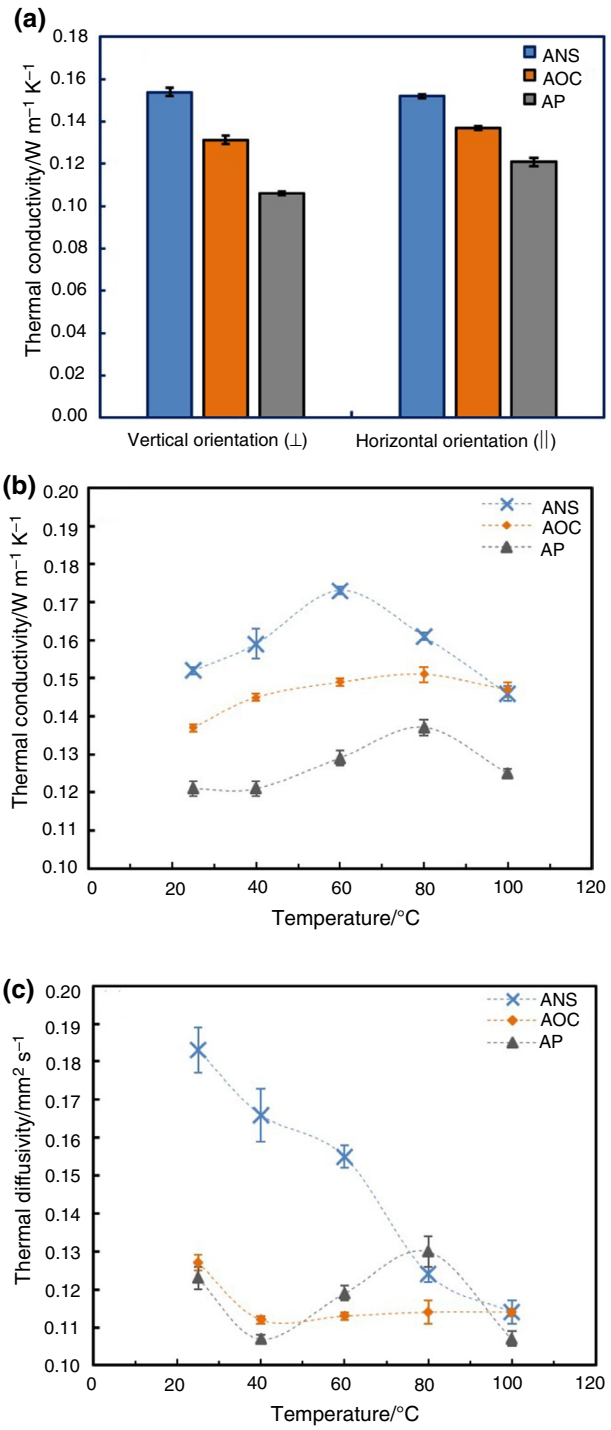

Fig. 8 Thermal properties of AFRs: (**a**) thermal conductivity at 25 °C, (**b**) and (**c**) thermal conductivity and diffusivity at elevated temperature, respectively (measurement was made in the horizontal position)

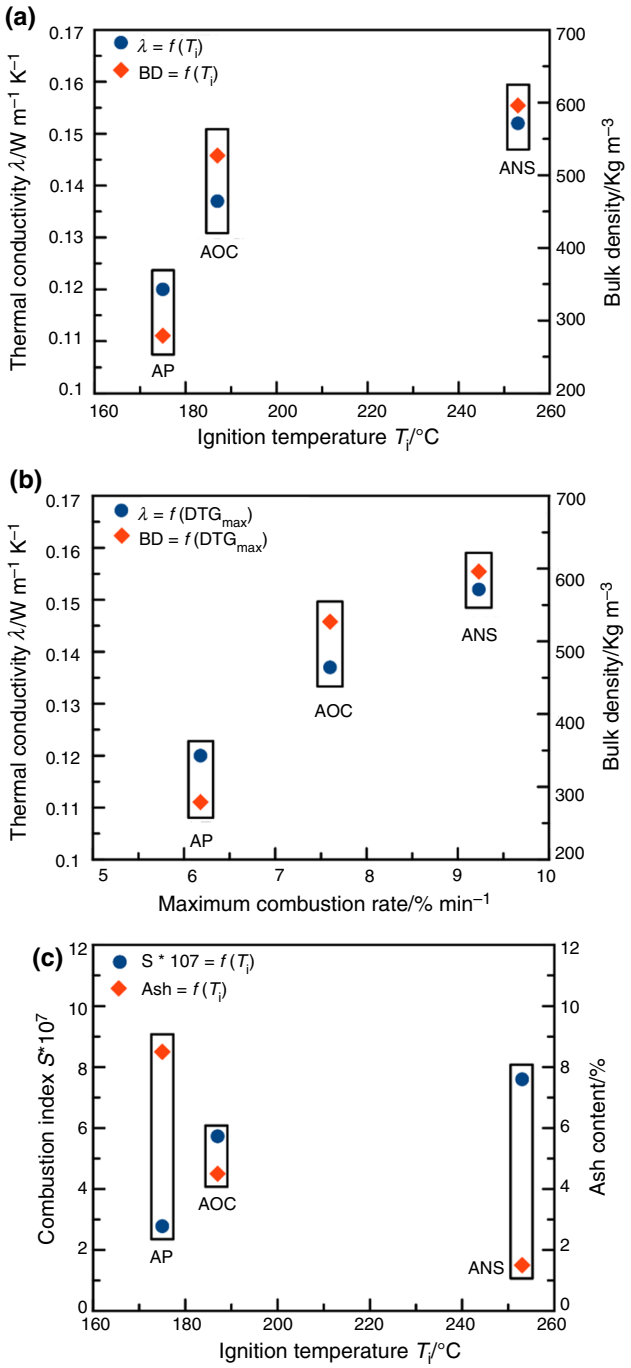

Fig. 9 Analysis of the most pertinent properties: (**a**) λ and BD against T_i, (**b**) λ and BD against maximum combustion rate, (**c**) combustion index and ash content against T_i

The opposite occurs for ANS associated with a higher conductive heat transfer. Looking more closely at the results in Fig. 9c, it is noteworthy that ANS, which has the lowest ash content (1.5%), has a higher ignition temperature and combustibility than AOC and AP.

The experimental results obtained from thermogravimetric analysis (TG and DTG) and thermal properties (by TPS technique) were consistent and found to be in agreement with the theoretical and experimental explanations given by Mansaray and Ghaly and Khalfi et al. [17, 43].

Summary and conclusions

This study has reported the physicochemical and thermal analysis of a new raw biomass, available in southwest Morocco for future biofuel production. Thermal analysis indicates that argan nut shell (ANS) is the most reactive material during pyrolysis compared to the other materials. Under oxidative conditions, three distinct phases can be distinguished in the thermal behavior of AFRs: drying, devolatilization and char oxidation. Again, ANS appears to be the most reactive material. Our results from thermogravimetric analysis and thermal properties analysis are consistent. We found that biomass with a lower thermal conductivity has a higher ignition temperature and may exhibit a lower rate of combustion. This behavior is also coherent with the literature results.

In conclusion, AP may cause problems of clogging in biomass combustion systems because of its high moisture and ash content and complex thermal degradation. AOC, with a higher oil and nitrogen content, will tend to produce high pollutant emissions during combustion. These features require the handling and pretreatment of AOC and AP biomass before direct thermochemical conversion. Otherwise, anaerobic digestion or fermentation could be an efficient way to valorize AOC and AP residues. Dried ANS, which has interesting values of HHV, FC/VM ratio, energy density, fuel reactivity and a negligible amount of nitrogen and ash content, appears to be the best alternative fuel for direct thermal conversion in combustion systems.

Acknowledgements The authors express their great thanks and appreciation to Dr. Ahmed IHLAL (LMER Agadir, Morocco) who allowed us to experiment the thermal properties of the studied biomasses at the hot disk facility. The financial support provided for this Project by the Region Centre Val de Loire, Project Code: VERA-P2 (No. 2015-00099702), is greatly appreciated.

References

1. Alain AV, Nasib Q, Hans PB, Yukawa H. Biomass to biofuels: Strategies for global industries. 1st ed. Amsterdam: Wiley; 2010.
2. Reddy BVS, Ramesh S, Ashok Kumar A, Wani SP, Ortiz R, Ceballos H, Sreedevi TK. Bio-fuel crops research for energy security and rural development in developing countries. BioEnergy Res. 2008;1:248–58.

3. Charrouf Z. Valorisation des produits de l'arganier pour une gestion durable des zones arides du sud-ouest marocain. Actes du 4ème Colloq Prod Nat d'origine végétale. 1999;195–209.
4. Nill D, Böhnert E. Value chains for the conservation of biological diversity for food and agriculture. 2006. pp. 37–50.
5. Zhar N, Naamani K, Dihazi A, Jaiti F, El Keroumi A. Comparative analysis of some biochemical parameters of argan pulp morphotypes (*Argania spinosa* (L.) skeels) during maturity and according to the continentality in Essaouira region (Morocco). Physiol Mol Biol Plants. 2016;22:361–70.
6. Charrouf Z, Hilali M, Jauregui O, Soufiaoui M, Guillaume D. Separation and characterization of phenolic compounds in argan fruit pulp using liquid chromatography-negative electrospray ionization tandem mass spectroscopy. Food Chem. 2007;100:1398–401.
7. Ait Laaziz S, Raji M, Hilali E, Essabir H, Rodrigue D, Bouhfid R, Qaiss A. Bio-composites based on polylactic acid and argan nut shell: production and properties. Int J Biol Macromol. 2017;104:30–42.
8. Rahib Y, Sarh B, Bostyn S, Bonnamy S, Boushaki T, Chaoufi J. Non-isothermal kinetic analysis of the combustion of argan shell biomass. Mater Today Proc. 2020;24:11–6.
9. Rahib Y, Elorf A, Sarh B, Bonnamy S, Chaoufi J, Ezahri M. Experimental analysis on thermal characteristics of argan nut shell (ANS) biomass as a green energy resource. Int J Renew Energy Res. 2019;9:1606–15.
10. Singh YD, Mahanta P, Bora U. Comprehensive characterization of lignocellulosic biomass through proximate, ultimate and compositional analysis for bioenergy production. Renew Energy. 2017;103:490–500.
11. Cai J, He Y, Yu X, Banks SW, Yang Y, Zhang X, Yu Y, Liu R, Bridgwater AV. Review of physicochemical properties and analytical characterization of lignocellulosic biomass. Renew Sustain Energy Rev. 2017;76:309–22.
12. Garcia R, Pizarro C, Lavin AG, Bueno JL. Biomass sources for thermal conversion. Techno-Econ Overv Fuel. 2017;195:182–9.
13. Vassilev SV, Baxter D, Andersen LK, Vassileva CG. An overview of the chemical composition of biomass. Fuel. 2010;89:913–33.
14. Obernberger I, Thek G. Physical characterisation and chemical composition of densified biomass fuels with regard to their combustion behaviour. Biomass Bioenergy. 2004;27:653–69.
15. Mansaray KG, Ghaly AE. Physical and thermochemical properties of rice husk. Energy Sources. 1997;19:989–1004.
16. El May Y, Jeguirim M, Dorge S, Trouvé G, Said R. Study on the thermal behavior of different date palm residues: characterization and devolatilization kinetics under inert and oxidative atmospheres. Energy. 2012;44:702–9.
17. Mansaray KG, Ghaly AE. Determination of reaction kinetics of rice husks in air using thermogravimetric analysis. Energy Sources. 1999;21:899–911.
18. Sjöström J, Blomqvist P. Direct measurements of thermal properties of wood pellets: elevated temperatures, fine fractions and moisture content. Fuel. 2014;134:460–6.
19. Zhu WK, Lin H, Cao Y, Li B. Thermal properties measurement of cut tobacco based on TPS method and thermal conductivity model. J Therm Anal Calorim. 2014;116:1117–23.
20. Lönnermark A, Persson H, Blomqvist P, Larsson I, Rahm M, Johan S. Small-scale methods for assessment of risk for self-heating of biomass pellets. SP Report; 2012.
21. Sait HH, Hussain A, Salema AA, Ani FN. Pyrolysis and combustion kinetics of date palm biomass using thermogravimetric analysis. Bioresour Technol. 2012;118:382–9.
22. Mann BF, Chen H, Herndon EM, Chu RK, Tolic N, Portier EF, Chowdhury TR, Robinson EW, Callister SJ, Wullschleger SD, Graham DE, Liang L. Indexing permafrost soil organic matter degradation using high-resolution mass spectrometry. PLoS One. 2015;10.
23. Loo S V, Koppejan J. The handbook of biomass combustion and co-firing. Earthscan; 2008. pp. 7–14.
24. Reis JS, Araujo RO, Lima VMR, Queiroz LS, da Costa CEF, Pardauil JJR, Chaar JS, Rocha Filho GN, de Souza LKC. Combustion properties of potential Amazon biomass waste for use as fuel. J Therm Anal Calorim. 2019;138:3535–9.
25. Li XG, Ma BG, Xu L, Hu ZW, Wang XG. Thermogravimetric analysis of the co-combustion of the blends with high ash coal and waste tyres. Thermochim Acta. 2006;441:79–83.
26. Paniagua S, Calvo LF, Escapa C, Coimbra RN, Otero M, García AI. Chlorella sorokiniana thermogravimetric analysis and combustion characteristic indexes estimation. J Therm Anal Calorim. 2018;131:3139–49.
27. Pratap A, Sharma K. Applications of some thermo-analytical techniques to glasses and polymers. J Therm Anal Calorim. 2012;107:171–82.
28. Berge A, Adl-Zarrabi B, Hagentoft CE. Determination of specific heat capacity by transient plane source. Front Archit Res. 2013;2:476–82.
29. Bu C, Leckner B, Chen X, Pallarès D, Liu D, Gómez-Barea A. Devolatilization of a single fuel particle in a fluidized bed under oxy-combustion conditions. Part A Exp Res Combust Flame. 2015;162:797–808.
30. Gil MV, Casal D, Pevida C, Pis JJ, Rubiera F. Thermal behaviour and kinetics of coal/biomass blends during co-combustion. Bioresour Technol. 2010;101:5601–8.
31. Yi Q, Qi F, Cheng G, Zhang Y, Xiao B, Hu Z, Liu S, Cai H, Xu S. Thermogravimetric analysis of co-combustion of biomass and biochar. J Therm Anal Calorim. 2013;112:1475–9.
32. Koukouch A, Idlimam A, Asbik M, Sarh B, Izrar B, Bostyn S, Bah A, Ansari O, Zegaoui O, Amine A. Experimental determination of the effective moisture diffusivity and activation energy during convective solar drying of olive pomace waste. Renew Energy. 2017;101:565–74.
33. Folayan AJ, Anawe PAL. Synthesis and characterization of Argania spinosa (Argan oil) biodiesel by sodium hydroxide catalyzed transesterification reaction as alternative for petro-diesel in direct injection, compression ignition engines. Heliyon. 2019;5:e02427.
34. Abdelaziz M, Aouda N, Mahdi KZ. In vitro estimate of the energy value of *Argania spinosa* L. from Algeria. Livest Res Rural Dev. 2014;26.
35. Elabed A. Réactivité thermique et cinétique de dégradation du bois d'arganier Application à l'élaboration de charbon actif par activation chimique à l'acide phosphorique. Mohammed V–Agdal; 2007. pp. 83–7.
36. Shah MA, Khan MNS, Kumar V. Biomass residue characterization for their potential application as biofuels. J Therm Anal Calorim. 2018;134:2137–45.
37. Essabir H. Bio-composites à base de coque de noix d'arganier: Mise en œuvre, caractérisation et modélisation du comportement mécanique. Ibn Zohr; 2014. pp. 76–86
38. Suleiman BM, Larfeldt J, Leckner B, Gustavsson M. Thermal conductivity and diffusivity of wood. Wood Sci Technol. 1999;33:465–73.
39. Ai Q, Hu ZW, Liu M, Xia XL, Xie M. Influence of sensor orientations on the thermal conductivity measurements of liquids by transient hot disk technique. J Therm Anal Calorim. 2017;128:289–300.
40. Tatane M, Elminor H, Ayeb M, Lacherai A, Feddaoui M, Aitnouh F, Boukhattem L. Effect of argan nut shell powder on thermal and mechanical behavior of compressed earth blocks. Int J Appl Eng Res. 2018;13:4740–50.

41. Adl-Zarrabi B, Boström L, Wickström U. Using the TPS method for determining the thermal properties of concrete and wood at elevated temperature. Fire Mater. 2006;30:359–69.
42. Kayode CA. Ludwig's applied process design for chemical and petrochemical plants. 4th ed. Amsterdam: Elsevier; 2007. p. 103–109.
43. Khalfi A, Trouvé G, Delfosse L, Delobel R. Influence of apparent density during the burning of wood waste furniture. J Fire Sci. 2004;22:229–50.